Theoretical Assessment of Ice Loading of Cables as a Function of their Torsional Stiffness

C. Hardy[1], A. Leblond[2] and D. Gagnon[3]

[1]Claude Hardy International Inc., Canada, chardy@sympatico.ca
[2]Hydro-Québec TransÉnergie, Canada, leblond.andre.2@hydro.qc.ca
[3]Hydro-Québec, IREQ, Canada, gagnon.daniel@ireq.ca

***Abstract*—This paper deals with a 2-D numerical modeling of ice accretion on aerial cables and conductors. This model, which is then extended approximately to cover actual 3-D cases, is developed on a non-dimensional basis so that results can be easily transposed to a wide variety of ice density, span length, cable diameter and torsional stiffness. The model is used to predict the shape and volume of the accretion as a function of the ice precipitation height and the cable torsional stiffness. It is demonstrated that the ice load is always comprised between two limits resulting from accretion on a fixed rigid cylinder on the low side and a freely rotating cylinder on the high side, with actual cases standing in between according to decreasing torsional stiffness. It is also shown accordingly that spacered conductor bundles are much less prone to severe icing than similar single conductors.**

I. Introduction

It is generally recognized that accretion of ice on aerial cables is affected by their aptitude to twist under eccentric loading which, in turn, depends on their torsional stiffness. As a matter of fact, the profile of the ice accretion at any given point along the span and at any given time is determined by the history of rotation at this point since the beginning of the precipitation event. It is known from experience that this profile can follow a variety of convex shapes from a fully eccentric crescent in the case of very stiff cables to a quasi-concentric circle in the case of torsionally flexible cables.

Predicting accurately the ice load on a cable system can only be done on the basis of a model that can reproduce the actual profile of the ice sleeves in contrast to most common icing models which assume a simple, invariable profile such as a semi-elliptic profile [1], a concentric circular profile [2] or a 3-quadrant spiral profile [3].

In other respects, it is quite difficult to generate the information solely from field tests as in [4] since significant icing precipitations are rare. Besides, as it is also the case for icing tests [5] in a wind tunnel, the data cannot be easily extrapolated to different cable systems.

In consideration of this situation, this paper deals with the development of an appropriate 2-D model which takes into account the cable torsional stiffness. This 2-D model which is then extended approximately to 3-D yields the rotation of the cable as well as the shape and volume (or weight) of the accretion as a function of precipitation.

II. 2-D Modeling

A. Basic Assumptions

Before proceeding to the formulation of the present cable icing model, it is important to state the basic assumptions upon which it stands. Hence, it is assumed that:

- Ice accretes only on the face of the cable exposed to precipitation and on this face, the accretion grows in the direction of the precipitation only, not sideways.
- Liquid precipitation transforms immediately and completely into solid ice accretion as it hits the cable (dry accretion only).
- Ice density is everywhere uniform.
- The precipitation angle with respect to vertical is invariable during a given ice storm.
- The torsional stiffness of the ice sleeve is much lower than the torsional stiffness of the cable and, as a result, it can be neglected.

Besides, it should be noted that the expression “icing precipitation height” will be used throughout this paper meaning the thickness of the ice accretion on a flat surface perpendicular to the precipitation.

B. First Limit Case: Fixed Rigid Cylinder

The simplest limit case is represented by a rigid circular cylinder with outer radius r_0 and length L fixed at the ends. In such a case, the volume V of the accretion may be expressed as:

$$V=2r_0hL \tag{1}$$

where h is the icing precipitation height. This volume would be identical should the ice accrete on a flat surface of area $2r_0L$ perpendicular to the precipitation. The shape of the ice sleeve is depicted in Fig. 1. The equivalent radial thickness (r-r_0) of this sleeve may be determined from the following expression:

$$r - r_0 = r_0 [(1+2h/\pi r_0)^{1/2}-1] \quad (2)$$

where r is the radius of the ice sleeve.

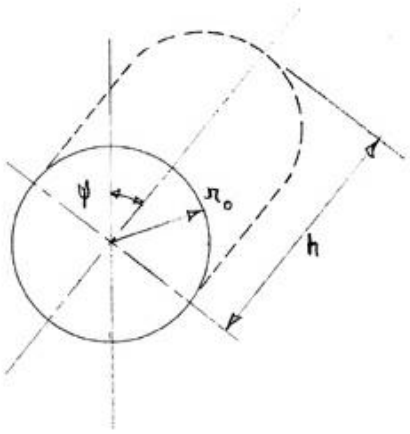

Fig. 1. Geometric contour of the accretion on a fixed rigid cylinder.

C. Second Limit Case: Free Rotating Rigid Cylinder

The other limit case is represented by a free rotating circular cylinder, which is equivalent to a cylinder that could not oppose any significant resistance to the torque exerted by the eccentric ice load. The torque exerted by the wind load on the ice-covered cable is not considered here. In such a case, the ice accretion builds up uniformly and concentrically around the cylinder. With dh designating the increment of icing precipitation height while the cylinder makes a complete turn and r, the current radius of the ice sleeve, the following equation:

$$2rdh = 2\pi rdr \quad (3)$$

expressing conservation of volume must be satisfied. Integrating this equation from the initial condition $r = r_0$ yields:

$$r = r_0 + h/\pi \quad (4)$$

Hence, it comes out that the radial thickness (r-r_0) of the ice sleeve is solely a function of the precipitation height and it is independent of the cylinder diameter. The corresponding volume of this concentric ice sleeve may be expressed as:

$$V = (2r_0h + h^2/\pi)L \quad (5)$$

This expression is important as it provides the upper limit of the volume of the accretion or, equivalently the ice load, that can build on a circular cylinder or cable. It may be noted that the first term on the right hand side corresponds to the lower limit, i.e. to the basic ice load on a fixed rigid cylinder as per (1) above, while the second term translates the overload due to the free rotation of the cylinder. The ratio of this overload to the basic ice load is directly proportional to precipitation height h. When the precipitation height reaches $2\pi r_0$, the basic ice load doubles as a result of the cylinder rotation.

D. Generic Case: Spring-Mounted Rigid Cylinder

Let us imagine, as illustrated in Fig. 2, a rigid circular cylinder mounted on a torsional spring at each end that is exposed to icing precipitation coming down at an angle ψ with the vertical. Let us define three orthogonal systems of axes: system uOv which is fixed and lined up with the horizontal and the vertical respectively; system xOy which is also fixed but lined up along the direction of the precipitation and, finally, system $XXOYY$ which rotates with the cylinder while angle ϕ denotes its angular position with respect to fixed axis Ov.

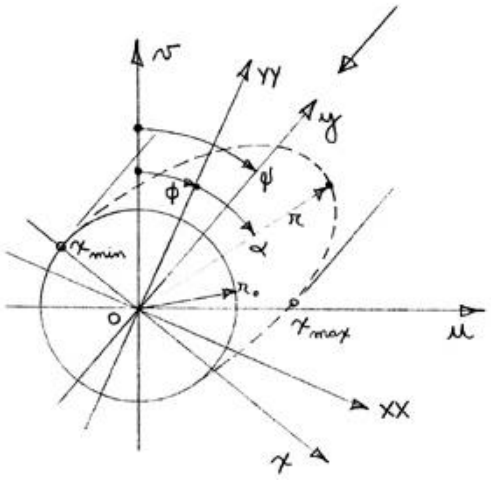

Fig. 2. Coordinates systems definition for cylinder accretion.

Let us also consider that the ice accretion process occurs incrementally, a new layer of ice of thickness dh accreting on the exposed face of the cylinder for each increment of time. Defining angle β_{ij} as:

$$\beta_{ij} = \phi_i + \alpha_{ij} - \psi \quad (6)$$

where sub-index i refers to increment order while sub-index j refers to any generic point on the periphery of the accretion, coordinates x_{ij} and y_{ij} in the xOy system may be expressed as follows:

$$x_{ij} = r_{ij} \sin \beta_{ij} \quad (7)$$

$$y_{ij} = r_{ij} \cos \beta_{ij} \quad (8)$$

Following an incremental accretion of thickness dh, but prior to the resulting incremental rotation, these coordinates transform into:

$$x_{i+1/2,\,j} = x_{ij} \quad (9)$$

$$y_{i+1/2,\,j} = y_{ij} + dh \quad (10)$$

where sub-index i+1/2 stands for the current status of the accretion process. On the non-exposed side, the current coordinates of the periphery stay unchanged. The incremental

volume dV of the accretion may be determined from:

$$dV_{i+1}=Ldh(x_{max} - x_{min}) \tag{11}$$

where, as depicted in Fig. 2, x_{max} and x_{min} denote the farthermost points on the periphery of the ice sleeve along a direction perpendicular to the precipitation. This incremental volume dV_{i+1} then adds up to the previous total volume V_i to yield the current total volume V_{i+1}.

It is now appropriate to work out the current position of the center of gravity of the ice sleeve in order then to balance the torque exerted by the eccentric ice load against the spring restoring torque. Referring to Fig. 3, let us consider element PP'Q'Q spanning stations j and j+1 on the incremental layer of accreted ice. In the fixed xOy system of axes, the center of gravity of this element is easily determined. Integration over the whole stretch of this incremental layer then provides the coordinates $\bar{x}_{i+1/2}$, $\bar{y}_{i+1/2}$ of its center of gravity :

$$\bar{x}_{i+1/2} = \frac{1}{2} dhL \left[\sum_{x_{\min}}^{x_{\max}} \left(x^2{}_{i+1/2,j+1} - x^2{}_{i+1/2,j} \right) \right] / dV_{i+1} \tag{12}$$

$$\bar{y}_{i+1/2} = \frac{1}{2} dhL \left[\sum_{x_{\min}}^{x_{\max}} \left(x_{i+1/2,j+1} - x_{i+1/2,j} \right) * \left(y_{i+1/2,j+1} - y_{i+1/2,j} \right) / dV_{i+1} \right] \tag{13}$$

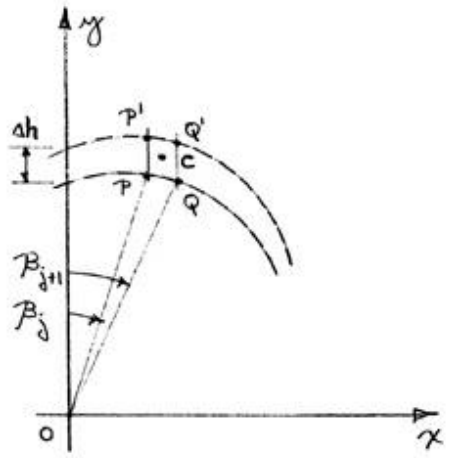

Fig. 3. Incremental accretion element in the xOy coordinate system.

Continuing, the updated coordinates $\bar{X}_{i+1/2}$, $\bar{Y}_{i+1/2}$ of the center of gravity of the whole ice sleeve, before incremental rotation, may be calculated as follows:

$$\bar{X}_{i+1/2} = \left(V_i \bar{X}_i + dV_{i+1} \bar{x}_{i+1/2} \right) / V_{i+1} \tag{14}$$

$$\bar{Y}_{i+1/2} = \left(V_i \bar{Y}_i + dV_{i+1} \bar{y}_{i+1/2} \right) / V_{i+1} \tag{15}$$

which may then be substituted into the following relationships:

$$\overline{XX}_{i+1/2} = \bar{X}_{i+1/2} \cos(\psi - \phi_i) + \bar{Y}_{i+1/2} \sin(\psi - \phi_i) \tag{16}$$

$$\overline{YY}_{i+1/2} = -\bar{X}_{i+1/2} \sin(\psi - \phi_i) + \bar{Y}_{i+1/2} \cos(\psi - \phi_i) \tag{17}$$

and, in turn, into:

$$\bar{r}_{i+1/2} = (\overline{XX}^2{}_{i+1/2} + \overline{YY}^2{}_{i+1/2})^{1/2} \tag{18}$$

$$\bar{\alpha}_{i+1/2} = \mathrm{tg}^{-1}(\overline{XX}_{i+1/2} / \overline{YY}_{i+1/2}) \tag{19}$$

to get the polar coordinates $\bar{r}_{i+/2}$, $\bar{\alpha}_{i+/2}$ of the center of gravity of the current ice sleeve in the fixed $XXOYY$ coordinate system. The torque T_{i+1} exerted by this eccentric ice sleeve under the action of gravity may then be expressed as:

$$T_{i+1} = \rho V_{i+1} \bar{r}_{i+1/2} \sin(\bar{\alpha}_{i+1/2} + \phi_{i+1}) \tag{20}$$

where ρ is the density of the accreted ice. This torque must be balanced by the restoring torque $k\phi_{i+1}$ put up by the torsional springs set up at the ends, a condition that translates into the following equilibrium equation:

$$\phi_{i+1} = (\rho V_{i+1} \bar{r}_{i+1/2} / k) \sin(\bar{\alpha}_{i+1/2} + \phi_{i+1}) \tag{21}$$

which has to be solved for the current rotation ϕ_{i+1} of the cylinder.

Once ϕ_{i+1} has been determined, the coordinates of the center of gravity of the ice sleeve may be updated using the following expressions:

$$\bar{X}_{i+1} = \bar{r}_{i+1/2} \sin(\bar{\alpha}_{i+1/2} + \phi_{i+1} - \psi) \tag{22}$$

$$\bar{Y}_{i+1} = \bar{r}_{i+1/2} \cos(\bar{\alpha}_{i+1/2} + \phi_{i+1} - \psi) \tag{23}$$

As for the current coordinates of the points on the periphery of the ice sleeve, they may be calculated by means of the following relationships:

$$r_{i+1,j} = r_{i+1/2,j} = (x^2{}_{i+1/2,j} + y^2{}_{i+1/2,j})^{1/2} \tag{24}$$

$$\beta_{i+1/2,j} = \mathrm{tg}^{-1}(x_{i+1/2,j} / y_{i+1/2,j}) \tag{25}$$

$$\beta_{i+1,j} = \beta_{i+1/2,j} + \phi_{i+1} - \phi_i \tag{26}$$

$$x_{i+1,j} = r_{i+1} \sin \beta_{i+1,j} \tag{27}$$

$$y_{i+1,j} = r_{i+1} \cos \beta_{i+1,j} \tag{28}$$

Now, before proceeding to computation, it is highly advantageous to convert all equations to a non-dimensional format. This normalization is done through the reduction of dimensional variables by means of the cylinder radius r_0. For instance:

$$x^* = x/r_0 \; ; \quad h^* = y/r_0 \; ; \ldots \text{etc.} \tag{29}$$

In this context, the reduced volume V^* of the accretion and the reduced torsional stiffness k^* are defined as:

$$V^* = V/(r^2{}_0 L) \tag{30}$$

$$k^* = k/(\rho\, r^3{}_0 L) \tag{31}$$

respectively. It may be seen that k^* integrates the accretion density ρ. Hence, a denser accretion translates into a decrease of the reduced torsional stiffness.

E. General Results

The above relationships have been programmed and solved by means of a specialized commercial software. Hence, the cylinder periphery has been divided into 90 four-degrees sectors and the icing precipitation has been applied at a rate varied between 0.1 r_0 and 0.4 r_0. Figure 4 shows the evolution of the accretion shape for precipitation heights of 0, 2, 4, 6, 8 and 10 times the cylinder radius r_0, a reduced torsional stiffness k^* of 32 and a precipitation angle ψ of 45°. It may be observed that the ice sleeve takes a more circular shape as precipitation goes on and the cylinder rotates. It has also been noted that for lower torsional stiffness, the cylinder can make several turns about its central axis. In such cases, the ice sleeve gets ever more circular. Figure 5 illustrates the evolution of the ice shape for the same precipitation heights and angles as above but, this time, for a reduced torsional stiffness k^* increased four times to the value of 128. It may be observed now that the ice sleeve takes a more elongated shape, more or less aligned with the direction of the precipitation. At that point, due to its own weight, it tilts down appreciably, thus increasing the area of the exposed face all the more.

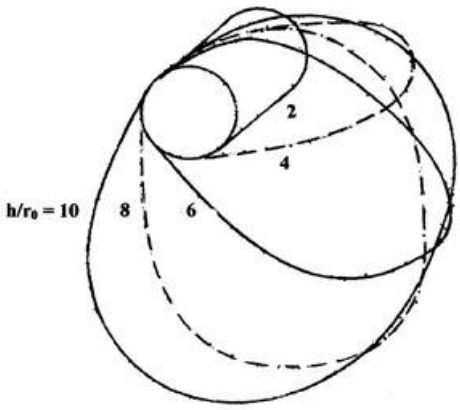

Fig. 4. Development of the contour of the accretion for a reduced torsional stiffness $k^* = 32$. Precipitation angle $\psi = 45^\circ$.

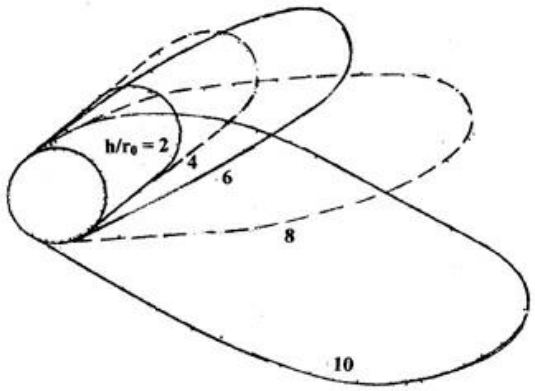

Fig. 5. Development of the contour of the accretion for a reduced torsional stiffness $k^* = 128$. Precipitation angle $\psi = 45^\circ$.

Figure 6 shows the reduced volume of the ice sleeve, a parameter proportional to the ice load, as a function of reduced precipitation height up to 10, for different reduced torsional stiffness ranging from 16 to 256. As a reference mark, it may be noted on the basis of (4) that the reduced precipitation height should go up to approximately 8 for the ice sleeve to reach a radial thickness of 45 mm on a rotating cylinder 35 mm in diameter. It is observed that, for a given precipitation height, the volume of the accretion increases as the torsional stiffness decreases. It is also found that the rate of growth of the ice sleeve increases all the way as the precipitation height increases. Also depicted in Fig. 6 are two curves corresponding to the volume of the ice accretion on a rotating rigid cylinder or equivalently, a rigid cylinder mounted on highly flexible torsional springs, identified $k^* = 0$, on the one part, and on a fixed rigid cylinder, or equivalently, a rigid cylinder mounted on highly stiff springs, identified $k^* >> 1$, on the other part. It may be seen that these two curves delimit a domain which encloses all the other curves corresponding to intermediate torsional stiffness. This confirms that the volume of the ice accretion or, equivalently, the ice load, reaches respectively a minimum on a fixed rigid cylinder and a maximum on a rotating rigid cylinder. The difference in the volume of accreted ice is entirely due to the rotation of the cylinder

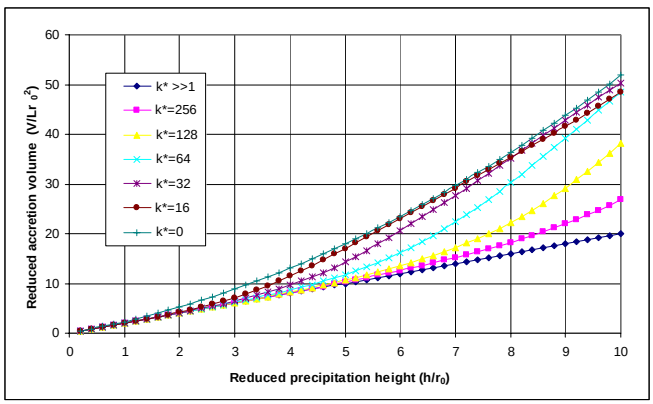

Fig. 6. Volume of the accretion as a function of precipitation height for different torsional stiffness.

To support that conclusion, Fig. 7 depicts the volume of the accretion as a function of the angle of rotation of the cylinder for four different reduced precipitation heights. It may be observed that each curve departs from a specific threshold value corresponding to a non-rotating cylinder and rises up to a specific ceiling value at angles of rotations of about 200° to 240°, thus converging to the freely rotating cylinder value.

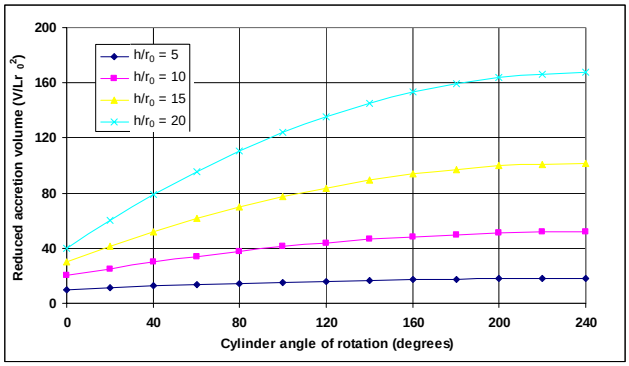

Fig. 7. Volume of the accretion as a function of the cylinder rotation for different precipitation heights.

Interestingly, it was found that the above curves may be expressed in a unified way through the following empirical relationships:

$$V^*\phi\, 2h^* + (h^{*2}/\pi)\sin(9\phi/22) \quad \phi < 220° \tag{32}$$

$$V^*\phi\, 2h^* + (h^{*2}/\pi) \quad \phi > 220° \tag{33}$$

The similarity between these last expressions and (5) is obvious, the first term on the right hand side representing the inevitable share of the accretion and the second term representing the share due to rotation.

III. 3-D MODELING

To work out a complete three-dimensional model which could be used to determine the evolution of the ice accretion as a function of precipitation along a flexible cable strung over a long span involves several difficulties. Such an exercise is out of the scope of this paper. Instead, the 3-D problem is approached in an approximate manner by means of the above 2-D numerical model, setting the torsional stiffness of the spring-mounted rigid cylinder in such a way as to yield a rotation equal to the average rotation of the cable along the span, under the influence of the same distributed torque, assumed to be uniform.

The rotation of a cable which is loaded by such a uniform torque τ due to the eccentric accretion of ice is governed by the following differential equation:

$$d^2\phi/ds^2 = -(\tau/GJ) \tag{34}$$

where s and GJ designate the coordinate along the cable axis and the cable torsional stiffness respectively. This equation is easily solved yielding for the rotation $\phi(s)$ of the cable along its central axis:

$$\phi(s) = (\tau/2GJ)(Ls - s^2) \tag{35}$$

where L is span length, and:

$$\phi_{mean} = \tau\, L^2/(12GJ) \tag{36}$$

stands for the average rotation ϕ_{mean} of the cable. Since the rotation of the spring-mounted rigid cylinder in the 2-D case writes:

$$\phi = \tau\, L/k_{eq} \tag{37}$$

it comes out that the equivalent torsional stiffness k_{eq} for the 2-D model may be expressed:

$$k_{eq} = 12GJ/L \tag{38}$$

IV. APPLICATION TO AERIAL CONDUCTORS AND GROUND WIRES

The above icing model will now be used to determine the propensity to icing of a single power conductor in relation to a single ground wire, on the one hand, and to a quad bundle of the same conductors, on the other hand.

A. Single Conductor Vs Single Ground Wire

The single ground wire to be looked at now for its relative propensity to icing is a 12.7 mm diameter, 7-wire steel strand which has been subjected to torsion tests on an outdoor test span [6] yielding a torsional stiffness of 24.9 Nm^2/rad. on the average. This stands at about 20% of the theoretical maximum torsional stiffness assuming the cable to behave as a solid, single-piece bar.

The conductor to be compared to is a Bersfort, a 35.6 mm diameter 48/7 ACSR (aluminum-conductor-steel-reinforced). For lack of a measured value as above, its actual torsional stiffness is assumed to take up as well 20% of its maximum value as a solid single-piece bar, i.e. GJ = 623 Nm^2/rad. The reduced equivalent torsional stiffness k_{eq}* of both cables may then be determined from the following expression:

$$k_{eq}^* = 12GJ/(\rho\, r^3{}_0\, L^2) \tag{39}$$

which results from the combination of (31) and (38). As applied to both cables for a span length ranging from 200 m to 400 m and glazing ice with a density of 8,82 kN/m^3, (39) yields close values for their reduced equivalent torsional stiffness, ranging from 3.32 to 0.83 for the ground wire and from 3.76 to 0.94 for the Bersfort conductor.

Hence, with reference to Fig. 6, it is obvious that with such a low torsional stiffness, both the ground wire and the Bersfort conductor would rotate almost freely under the influence of

any significant eccentric ice load and, as a result, would collect ice to a maximum. As (4) indicates, the radial thickness (r - r_0) of the quasi-circular ice sleeve would be the same on both cables for a given precipitation height. However, the resulting ice load on the Bersfort conductor would obviously be higher due to its larger diameter.

B. Single Conductor Vs Bundled Conductors

For power transmission lines operating at extra high voltage, twin, triple and quad bundled conductors are largely used. These bundles are usually fitted with spacers staggered along the span in order to maintain the geometry and control vibrations under adverse wind and ice effects. Such an arrangement, incidentally, results in a tremendous increase in the torsional stiffness of the system. This has to be taken into account when assessing the propensity of bundled conductors to icing. For instance, it may be demonstrated that for small rotations, the ratio of the torsional stiffness k_{bundle} of a quad bundle at a spacer to the torsional stiffness k_{single} of a single conductor of the same type may be written:

$$k_{bundle}/\, k_{single} = 2He^2/GJ + 4 \qquad (40)$$

where H designates the conductor tension and e the subconductor spacing. The first term on the right hand side results from the bundle effect on torsional stiffness while the second term corresponds to the four individual subconductors. Computed for icing conditions conducive to 50% and 75% of the 180 kN breaking load of the Bersfort conductors used in a quad bundle with 450 mm spacing, the above ratio comes out to 63 and 92 respectively.

Hence, in assessing the propensity of such a quad bundle to icing, it appears reasonable to consider the subconductors individually over one subspan length only as opposed to a full span length, as if, for all practical purpose, they could not rotate at the spacers. This way, their effective free length decreases quite significantly from 200 m to 400 m down to, typically, 40 m to 70 m. For such shorter lengths, the reduced equivalent torsional stiffness of the Bersfort conductor ranges from 94 and 27 approximately, according to (39).

Now, using Fig. 6 to interpolate the predicted volume of the accretion on a single subconductor for such an equivalent torsional stiffness and comparing to that of a single conductor used *in solo* yields Fig. 8. It may be observed that the predicted volume (or equivalently, load) of the accreted ice on a given conductor as used in a spacered quad bundle may be, in the shortest subspans, as low as 60% and, in the longest subspans, as low as 70% of the volume of ice accreted on a similar conductor as used *in solo*. That would occur for a reduced precipitation height h/r_0 of about 5 and 3 respectively translating a radial ice thickness of about 28 mm and 17 mm on the single Bersfort conductor. The relative lower propensity of the quad bundled conductors to icing decreases for higher precipitation heights but, yet, the ice load ratio may be as low as 70% in the shortest subspans for precipitation conducive to a 45 mm radial thickness of ice on the single conductor.

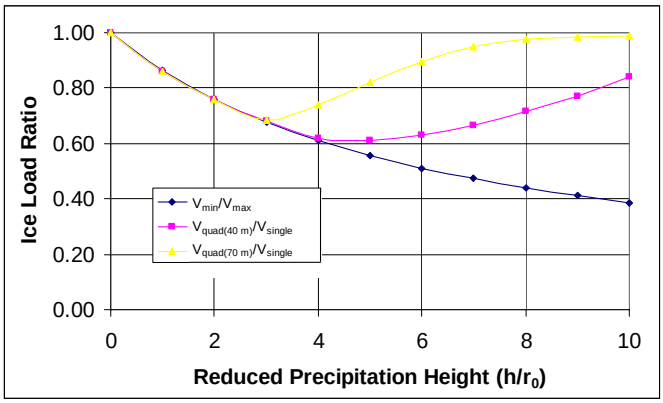

Fig. 8. Ratio of the ice load on a quad bundled conductor to the ice load on a similar single conductor as a function of precipitation height.

IV. CONCLUSION

It has been demonstrated by means of a dedicated numerical model that the propensity of cables to icing is bracketed within two limits translating accretion on a fixed rigid cylinder on the low side and a freely rotating cylinder on the high side. Using this model, it has been shown that power conductors and ground wires used *in solo* over usually long span lengths have an equivalent propensity to icing at an equivalent wind speed. As their torsional stiffness is low, both rotate almost freely on their central axis and as a result, collect maximum ice for any significant icing precipitation. In contrast, as a result of their much higher torsional stiffness, bundled conductors, which use a number of spacers staggered along the span, are less prone to icing than similar single conductors.

V. REFERENCES

[1] P.M. Chaîné and G. Castonguay, "New approach to radial ice thickness concept applied to bundle-like conductors", Study 4, Industrial Meteorology , Environment Canada, Toronto, 1974.

[2] K.F. Jones, "A simple model for freezing rain ice loads", in *Proc. of the 7th International Workshop on Atmospheric Icing of Structures*", Chicoutimi, Canada, 1996, pp. 412-416.

[3] P. McComber, "A non-circular accretion shape freezing rain model for transmission line icing", *9th International Workshop on Atmospheric Icing of Structures*", Chester, United Kingdom, June 2000.

[4] P. McComber, J. Druez and G. Sabourin, "A comparison of measured ice loads on ground wires, single and bundle conductors", *10th International Workshop on Atmospheric Icing of Structures*", Brno, Czech Republic, 2002.

[5] C. Blackburn, J.L. Laforte, D. Gagnon and M. St-Louis, "Comparative study of the quantity of rime and glaze accreted on free-rotating and fixed overhead ground cables", *10th International Workshop on Atmospheric Icing of Structures*", Brno, Czech Republic, 2002.

[6] "Mesure du couple de torsion", Attestation d'essais #53006461, Laboratoire Mécanique et Thermodynamique, IREQ, septembre 7, 2000.